Molecular Crystals and Liquid Crystals

ISSN: 1542-1406 (Print) 1563-5287 (Online) Journal homepage: http://www.tandfonline.com/loi/gmcl20

Nematic Defects and Colloids as Photonic Elements

M. Ravnik, M. Stimulak, M. Cancula & S. Zumer

To cite this article: M. Ravnik, M. Stimulak, M. Cancula & S. Zumer (2015) Nematic Defects and Colloids as Photonic Elements, Molecular Crystals and Liquid Crystals, 619:1, 61-69, DOI: 10.1080/15421406.2015.1087284

To link to this article: http://dx.doi.org/10.1080/15421406.2015.1087284

Mol. Cryst. Liq. Cryst., Vol. 619: pp. 61–69, 2015

ISSN: 1542-1406 print/1563-5287 online
DOI: 10.1080/15421406.2015.1087284

Taylor & Francis
Taylor & Francis Group

Nematic Defects and Colloids as Photonic Elements

M. RAVNIK,[1,*] M. STIMULAK,[1] M. CANCULA,[1]
AND S. ZUMER[1,2,*]

[1]Faculty of Mathematics and Physics, University of Ljubljana, Slovenia
[2]Jozef Stefan Institute, Slovenia

Birefringent structures in liquid crystalline fluids, such as colloidal assemblies or topological defects, show high potential for use as photonic elements. Here, we present a brief overview of two photonic phenomena originating from coupling light fields with complex birefringent nematic profiles: (i) the generation of vector laser beams from simple Gaussian beams by propagating light along nematic discliantions, and (ii) tunable photonic crystals from blue phase colloidal crystals conditioned by the different underlying symmetries of the particle lattice and the blue phase birefringence. The polarization profile of initially simple linearly polarized Gaussian beams is shown to change into a defect structure at distinct distances travelled along the disclination with the topological invariant (winding number) of the light field and nematic director distinctly coupled. Upon pulsed laser illumination, the nematic discliantions are also shown to split the light pulse into multiple intensity regions. Blue phase I face centred cubic colloidal crystals are shown as examples of tunable photonic crystals, where local band-baps can open by differently combining the symmetries of the two components, e.g. by changing the particle size. The spatial profiles of selected photonic bands in the blue phase colloidal crystals are shown, finding the particles and blue phase double twist cylinders as possible carriers of high-light-intensity regions.

Keywords photonic crystals; defects; colloidal crystals; nematic liquid crystals; blue phases; photonic crystal

1. Introduction

Creating novel complex profiles of birefringence by soft liquid crystalline structures is an interesting approach towards controlling the flow-of-light at the microscopic level [1, 2, 3, 4, 5, 6]. The key differentiator of such approach is that the materials are soft, liquid, possibly polymerisable, multicomponent, and well responsive to external fields, including electric and light, which allows for typically highly tunable and well controllable manipulation of the light [7, 8, 9, 10]. This area of research includes systems ranging from colloidal nematic dispersions [11, 12, 13], nano-scribed micro-patterns and cavities [14], to polymer template composites [15, 16] and complex birefringent phases, including cholesteric blue

This is a joint paper for the two invited talks Nematic disclinations as waveguides (Zumer) and Photonic structures from nematic colloidal tilings and blue phase colloids (Ravnik).

*Address correspondence to M. Ravnik or S. Zumer, Faculty of Mathematics and Physics, University of Ljubljana, Slovenia. E-mail: miha.ravnik@fmf.uni-lj.si, slobodan.zumer@fmf.uni-lj.si

Color versions of one or more of the figures in the article can be found online at www.tandfonline.com/gmcl.

phases [17, 18]. From more applied perspective, this work is in the direction of creating novel metamaterial, plasmonic and photonic crystal components [19, 20, 21].

Recent directions in the research of complex structures based on liquidcrystalline components include toplogical colloids [3, 22], unconventional elasticity materials [23, 24, 25], chiral nematic based profiles [26], complex particle-shape design [4, 27], topological charge templates [28], quasicrystalline patterns [29, 26], active liquid crystals [30], and droplet shape control [7], which allow for new soft matter photonic elements such as cholesteric lasers [31], negative refraction setups [32], droplet resonators [2], filament wave guides [10], and plasmonic polarizers [33]. At the core of these elements is the large and well-tunable birefringence of the liquid crytstalline elements, which is responsive at time-scales ranging from milliseconds to femtoseconds and spatial scales ranging from micrometers to nanometers.

Our motivation is in modelling the coupling and response of light field to the complex birefringent liquid crystal-based structures [34, 35]. There is a notable selection of techniques in the literature that can be used to model light propagation in birefringent medium, with the prime examples the Jones method [36] and the Berreman method [37]. More recent, and typically also much more computationally intensive methods include solvers of photonic eigenstates [38, 39], such as for calculating photonic bands, and direct time solvers of Maxwell's equations, like finite difference time domain methods [40].

In this contribution, we give a brief overview of our two approaches towards nematic soft matter photonics. As the first contribution, we explain the laser beam propagation –continuous and pulsed- along nematic disclinations and demonstrate the coupling between the polarization profile and the nematic director [35]. As the second contribution we show the tuning of photonic bands in the blue phase colloidal crystals [34], as a showing example of soft multicomponent material with different underlying symmetries that condition the photonic response. Also, we show the spatial profile of the selected photonic bands which reveals the high and low-light–intensity regions in such anisotropic photonic crystals.

2. Methods and Theory

A strong method for modelling nematic structures is by using numerical calculations based on the free energy minimization [41, 42]. This mesoscopic method typically relies on nematic order parameter tensor Q_{ij} and Landau-de Gennes free energy. It is used by several groups worldwide and was shown to give reliable results and even quantitative agreement with experiments. From photonics perspective, the order parameter tensor Q_{ij} is directly related to the nematic permittivity tensor ε_{ij} as:

$$\varepsilon_{ij} = \bar{\varepsilon}\delta_{ij} + \frac{2}{3}\varepsilon_a^{mol} Q_{ij}, \tag{1}$$

where $\bar{\varepsilon}$ is the average electric permittivity and ε_a^{mol} is the molecular dielectric anisotropy,both at optical frequencies when considered in photonics. Therefore, being able to model nematic ordering via nematic order parameter tensor also provides full information about the permittivity profile and the resulting birefringence. We approach the photonic response of nematic structures by two complementary approaches: (i) Finite Difference Time Domain (FDTD) simulations [40, 35] and (ii) photonic band calculations [38, 34].

The FDTD simulations simulate the time-evolution of the light-field -i.e. the electric ($\boldsymbol{E}$) and magnetic ($\boldsymbol{H}$) fields - as given by the time-dependent Maxwell's equations. More specifically, starting from given initial field profile in space and time, the light field components are propagated on a discrete (cubic) mesh, which has to be properly conditioned to assure stability [43]. In the presented results, we assume no free charges and no currents and isotropic magnetic permeability of the liquid crystal. The calculations are performed on parallelized CPU or GPU platform, typically, with simulation boxes of few 100 × few 100 × few 100 and 100 thousand time steps, which requires about 1 day per calculation. A notable advantage of our developed approach is that it also allows for mutual coupling between the light and nematic field, which can become important in particular at high light intensities.

The photonic band calculations are used to explore the propagation modes of light in periodic patterns on nematic birefringence. The approach is fully analogous to the calculation of electron bands in classical semiconductors, and starts with the Bloch theorem function for the optical bands where the proper selection of the local basis is a notable advantage to assure transversality condition of the light field, i.e. to comply with the $\nabla \cdot (\underline{\varepsilon}\boldsymbol{E}) = 0$ and $\nabla \cdot \boldsymbol{H} = 0$ Maxwell's equations [44]. By using the Bloch ansatz function and Fourier transforming the dielectric permittivity tensor, effectively the photonic band calculations evolve into solving a distinct eigenproblem where the spatial (periodic) variation of the dielectiric permittivity tensor is the key defining variable of the problem. Directly solving the eigenproblem (e.g. for all eigenvalues) turns out to be computationally demanding and typically, only rather small simulation boxes can be considered (e.g. 20×20×20); therefore, using iterative solvers for the eigenproblem are generally needed, for example as in Ref 39.

3. Generation of Light Beams with Nematic Disclination Lines

We find that nematic disclination lines can be used for generating vector light beams with various intensity, polarization and phase profiles by performing FDTD numerical calculations [35]. When a Gaussian laser beam with linear polarization propagates along a disclination line its polarization and intensity profiles change (see Fig. 1). A zero-intensity region appears at the defect core, where the director is undefined and the dielectric permittivity becomes locally isotropic. The intensity profile in shown in the top half of Fig. 1, where the formation of zero-intensity region is observed; additionally, the polarization of the light beam undergoes interesting changes. At a distinct length travelled along the disclination z_d the original linear polarization transforms into a radial polarization, notably with the central defect. Indeed, it can be shown more generally, that the winding number (charge) of the defect in polarization profile is always equal to twice the winding number of the liquid crystal defect, as illustrated in the bottom panels of Fig. 1. The distinct distances at which the defect in polarization emerges depend on the material birefringence Δn and light wavelength λ and are equal to

$$z_d = (2m + 1)\frac{\lambda}{2\Delta n}, \tag{2}$$

where m = 0,1,2 . . . Notably, the structure is periodic with a period of $\lambda/\Delta n$. A separate derivation using the Jones calculus confirms this relation; however, Jones simplified approach can not properly describe the intensity and polarization profiles at the axis of the beam. In our FDTD results and also from experiments, this is resolved by the intensity dropping to zero, as light refracts away from the defect core.

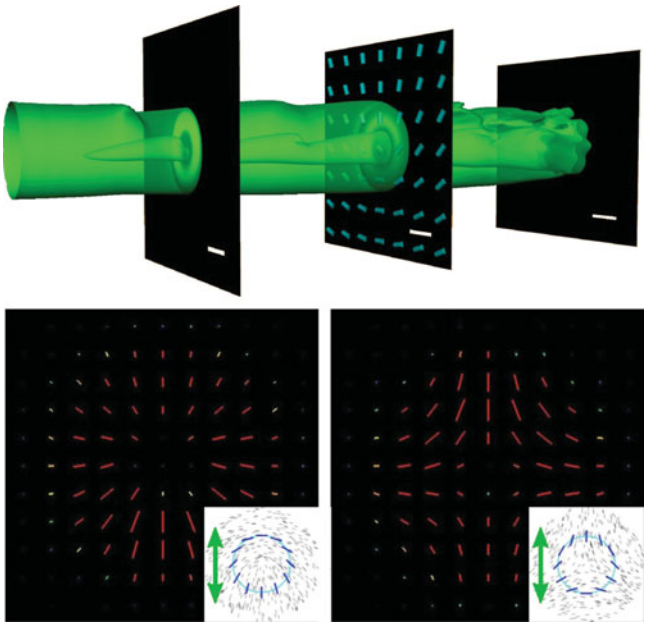

Figure 1. A continuous Gaussian laser light beam with initial linear polarization propagating along a nematic disclination line. The intensity profile of the beam (top) shows a zero- intensity region forming at the defect core, avoiding discontinuities in the light polarization. Blue cylinders show the liquid crystal director structure of a $+1/2$ disclination line. Bottom images show the polarization profiles at a certain distance z_d along disclinations with winding numbers $+1/2$ (left) and $-1/2$ (right), where polarization forms defects with winding numbers $+1$ and -1, respectively. Insets show the director profiles (dark blue lines) and incident light polarization (green two-headed arrows). The following numerical parameters are used in calculations: material birefringence 0.15, wavelength 480nm, lattice resolution 30nm, beam waist 1600 nm.

If the incident beam has circular rather than linear polarization, the defects in the polarization profile are again observed, but at different positions and with different winding numbers [35]. In this case, the winding number of the polarization defect is the same as that of the liquid crystal defect, interestingly, including half-integer winding numbers. Light polarization is closely tied to the electric field, which as a proper vector cannot form non-integer defects. However, this incompatibility is resolved by an additional half-integer-strength phase vortex at the axis. We thus show that disclination line couple the light's spin, angular orbital momentum, and the polarization profile.

Figure 2 presents the results for propagation of femtosecond laser pulses along disclination lines. As the incident linearly polarized light is a superposition of two polarization modes (ordinary and extraordinary), the pulse immediately splits into two modes with different propagation velocities. Each of the two modes then splits into multiple intensity regions, depending on the magnitude (but not the sign) of the disclination's winding number s, resulting in $4|s|$ separate regions. These regions and the corresponding polarization profiles are shown in Fig. 2. It can be seen that in one mode, the polarization is perpendicular to the director (ordinary), as in the other it is parallel (extraordinary), with dark spots where the orientation would be incompatible with the incident polarization. In the area between

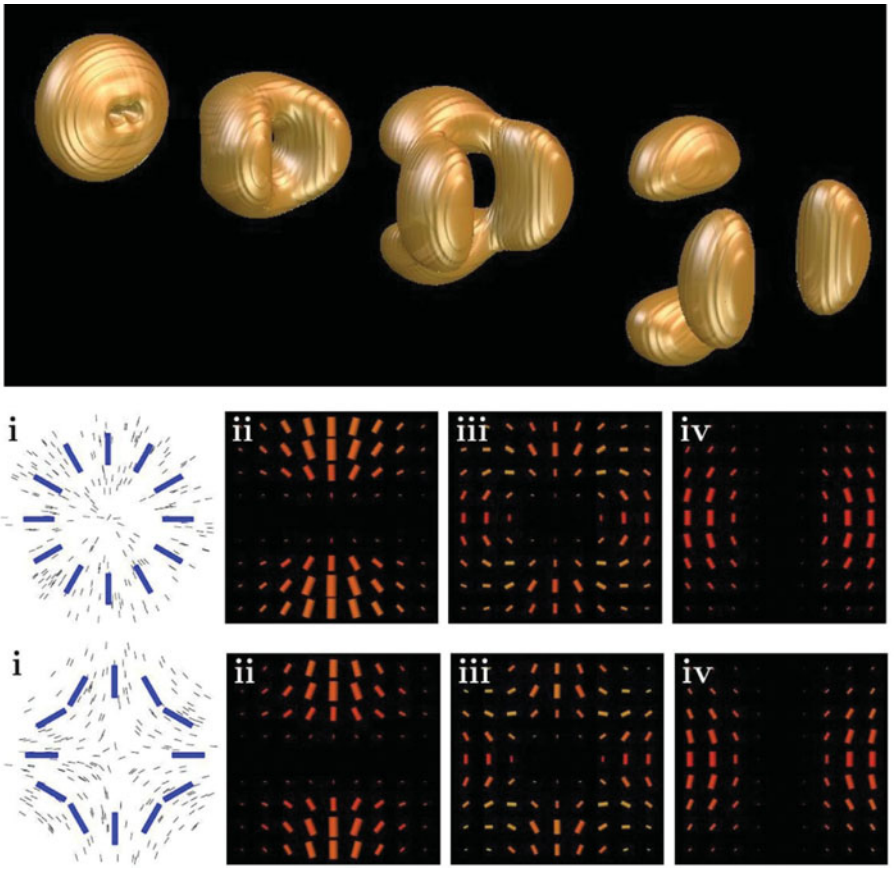

Figure 2. Propagation of a femtosecond laser pulse along a +/−1 nematic desclination line. (top) The light intensity profile shows the pulse splitting into four regions within two distinct planes, corresponding to ordinary and extraordinary polarization modes. In general, the pulse always splits into 4|s| parts in two planes, where s is the LC disclination winding number. Bottom images show two director profiles (i), as well as corresponding light polarization in the two planes (ii and iv) and between the planes (iii). The same numerical parameters as in Fig. 1 were used, while the pulse length was equal to 6fs.

the mode planes, the intensity is much lower, but a distinct defect pattern with twice the winding number of the disclination line can be observed, similar to those in the continuous illumination case.

4. Tunable Photonic Crystals from Blue Phase I FCC Colloidal Crystals

Photonic crystals require periodic variation of refractive index (dielectric permittivity) which can be in one, two or three spatial dimensions and is generally achieved by combining several components with different refractive index into a periodic array. In liquid crystals, however, the photonic crystal response can be achieved also by using a homogeneous material where the periodically spatially varying optical axis of the liquid crystal –the birefringence- effectively yields the periodic variation. The prime liquid crystalline

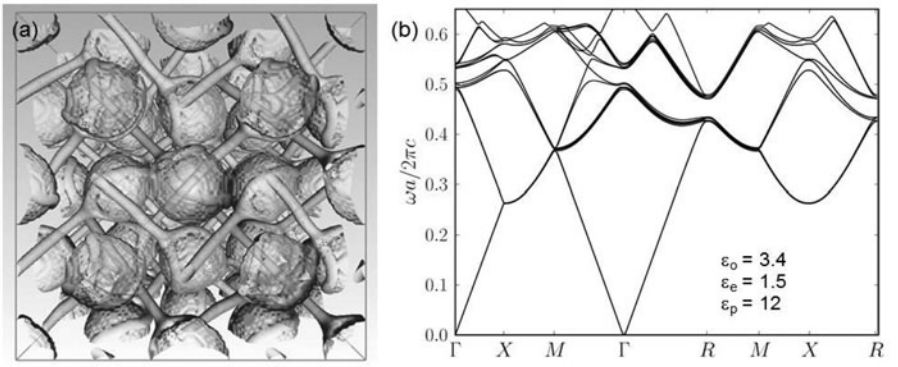

Figure 3. Blue phase I FCC colloidal crystals as photonic crystals. (a) Blue phase I colloidal crystals with 120 nm particles assembled into a face centred cubic lattice. (b) The corresponding photonic bands on the edge of the first irreducible Brillouin zone of a simple cubic symmetry, where ω is the eigenfrequency, a is the unit cell size, c is the speed of light and Γ, *X, M* and *R* are traditional wave vector points in the Brillouin zone.

materials with periodic birefringence are cubic cholesteric blue phases (blue phase I and II), which indeed were demonstrated to exhibit photonic crystal behaviour [44].

The idea of our work was to combine two different 'symmetries' of photonic crystals into one single material, and moreover, be able to tune the relevance of either of the two symmetries. Specifically, we consider chiral nematic blue I colloidal crystals [45, 46] and explore them as photonic crystal [34]. In these materials, the periodic defect network of the blue phases provides a regular array of trapping sites for colloidal particles which can stabilize a colloidal crysal. In blue phase I with inherent body centred cubic (BCC) symmetry, ∼100 nm sized particles organized into a face centred cubic (FCC) lattice have the lowest free energy (see Fig 3a). Therefore, effectively, the blue phase I FCC colloidal crystal combine the BCC symmetry of the blue phase with the FCC symmetry of the particle lattice into one photonic crystal material. New combined symmetry of such material is simple cubic (SC). Properties of such soft blue phase colloidal photonic crystals can be tuned by changing the elementary material properties of the blue phases, such as chirality and temperature, as well as of dielectric particles, such as dielectric constant, size and shape. Figure 3b shows photonic bands calculated for a BP I FCC colloidal crystal with 120 nm sized particles. We can see that multiple photonic bands are split apart, i.e. nondegenerate, as if compared to simple FCC structures in isotropic background (see Table 1), which is a direct consequence of anisotropic background. Specifically, photonic eigenfreqeuncies from three to eight calculated for wave vector Γ (i.e. k = (0,0,0)) are degenerated in FCC

Table 1. Eigenvalues of an FCC colloidal crystal with isotropic dielectric background (ε = 2.3). Particle sizes 120 nm, dielectric permittivity = 5. Note the degeneracy of frequencies from 3-8 and 9 and 10.

Eigenvalue number	1	2	3	4	5	6	7	8	9	10
ω a / 2π c	0	0	0.608	0.608	0.608	0.608	0.608	0.608	0.638	0.638

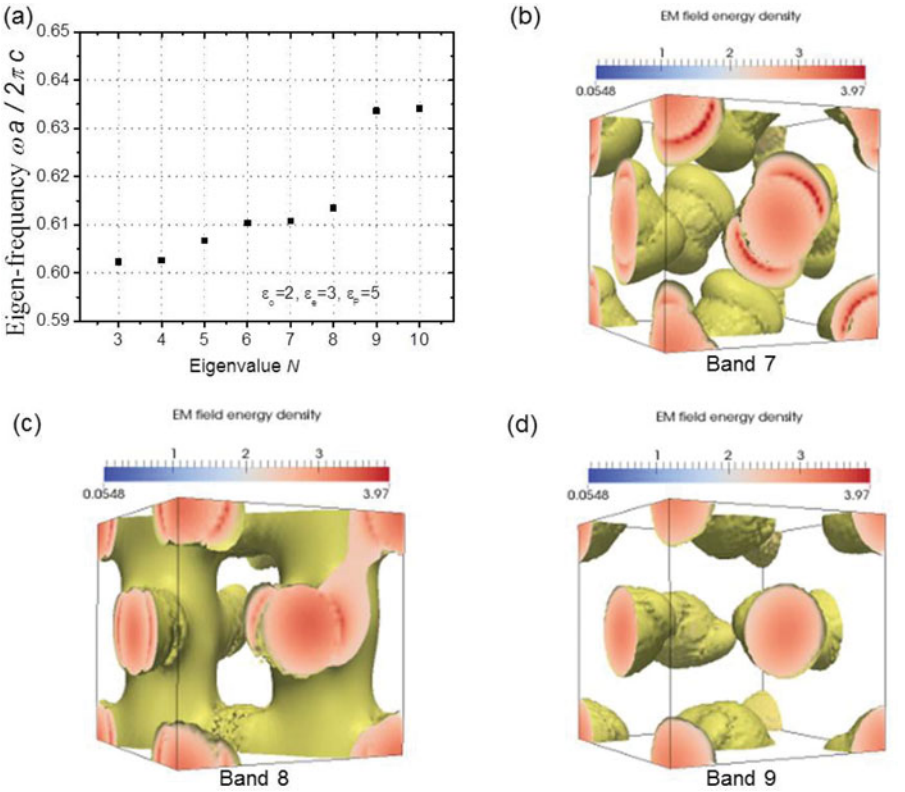

Figure 4. Eigen-frequencies and spatial profiles of selected photonic bands in BP I FCC colloidal crystal with 120 nmm sized particles. (a) First ten eigen-frequencies (the first and second are zero) for wave vector Γ (i.e. k = (0,0,0)). Note that eigen-frequencies from 3 to 8 are no longer degenerate, as if compared to degenerate values in FCC colloidal crystals with isotropic background (Table 1). Corresponding spatial profile of the (b) seventh, (c) eight and (d) ninth photonic band, visualized as regions of high electromagnetic field energy density (see ref 47). Calculations are performed for the following numerical parameters: ordinary LC dielectric permittivity $\varepsilon_o = 2$, extraordinary LC dielectric permittivity $\varepsilon_e = 3$ and isotropic dielectric permittivity of particles $\varepsilon_p = 5$, and particle diameter 120 nm.

photonic crystal with isotropic background (see Table 1) but are nondegenerate in the BP I FCC colloidal crystal (Fig 4a). With further consideration also new local bandgaps can open in the considered blue phase colloidal crystals [34], again as the result of competing symmetries of the blue phases and the particle lattice. The local photonic band gaps that appears from splitting degenerate states are typically in the range of $\Delta\omega/\omega \sim 2\%$. Figure 4b-d shows the spatial profiles of selected photonic bands in BP I FCC colloidal crystal, where strongly spatially different (orthogonal) bands indicate the possible emergence of a local band gap. In the presented bands, the high energy regions typically roughly coincide with particles and with distinct regions of blue phase profiles, interestingly the double twist cylinders (see Fig 4c). Finally, more broadly, these spatial profiles of photonic bands indicate that both particles as well as distinct patterns in liquid crystalline profiles, such as the double twist cylinders, could be considered and engineered as basic elements for photonic crystals.

5. Conclusions

In conclusion, we show selected examples of soft matter photonics: (i) the use of nematic discliantions as elements for shaping the polarization profile of simple (Gaussian) laser beams, and (ii) the performance of blue phase colloidal crystals as tunable photonic crystals. For nematic disclinations, we show that upon continuous illumination with linear laser beam, they can transform the initially linearly polarized simple beams into vector beams with winding number (charge) equal to twice the charge of the nematic dislination. Alternatively, if the initial beam is circularly polarized, vector beams with winding number equal to the winding number of the nematic disclinations emerge. Upon pulsed laser illumination of the disclinations, spatial splitting of the pulses is demonstrated. For blue phase colloidal crystals, their performance as tunable photonic crystals is explained where the combination of particle lattice symmetry and the symmetry of the blue phase birefringence mutually affect the photonic band structure. More generally, we show that soft nematic photonic crystals can join multiple components organized into differently symmetric structures which is a novel by-symmetry conditioned approach for tuning and designing photonic bands in photonic crystals. Finally, the demonstrated nematic photonic phenomena are explored as a possible new route towards controlling the flow of light at microscopic level via the design of soft-matter based photonic components, including lasers, light sources, resonators, switches, and waveguides.

6. Acknowledgments

The research was supported by the Slovenian Office of Science (ARRS, grants P1-0099 and Z1-5441). M. R. acknowledges support of the EC Marie Curie Program FREEFLUID.

References

[1] Hakobyan, D., & Brasselet, E. (2014), *Nat. Photon.*, *8*, 610–614.
[2] Humar, M., Ravnik, M., Pajk, S., & Musevic, I. (2009). *Nat. Photon.*, *3*, 595.
[3] Senyuk, B., Liu, Q., He, S., Kamien, R.D., Kusner, R. B., Lubensky, T. C., & Smalyukh, I. I. (2013). *Nature*, *493*, 200.
[4] Machon, T., & Alexander, G. P. (2013). *Proc. Natl. Acad. Sci. USA*, *110*, 14174.
[5] Tkalec, U., Ravnik, M., Copar, S., Zumer, S., & Musevic, I. (2011). *Science*, *333*, 62.
[6] Smalyukh, I. I., Lansac, Y., Clark, N.A., & Trivedi, R. P. (2010). *Nature Mat.*, *9*, 139.
[7] Peddireddy, K., Kumar, P., Thutupalli, S., Herminghaus, S., & Bahr, C. (2012). *Langmuir*, *28*, 12426.
[8] Coles, H., & Morris, S. (2010). *Nat. Photon.*, *4*, 676.
[9] Peccianti, M., Conti, C., Assanto, G., De Luca, A., & Umeton, C. (2002). *Appl. Phys. Lett.*, *81*, 3335.
[10] Peddireddy, K., Jampani, V. S. R., Thutupalli, S., Herminghaus, S., Bahr, C., & Musevic, I. (2013). *Opt. Exp.*, *21*, 30233.
[11] Poulin, P., Stark, H., Lubensky, T. C., & Weitz, D. A. (1997). *Science*, *275*, 1770.
[12] Yada, M., Yamamoto, J., & Yokoyama, H. (2004). *Phys. Rev. Lett*, *92*, 185501.
[13] Nych, A., Ognysta, U., Škarabot, M., Ravnik, M., Žumer, S., & Muševič, I. (2013). *Nat. Comm.*, *4*, 1489.
[14] Tasinkevych, M., Campbell, M. G., & Smalyukh, I. I. (2014). *Proc. Natl. Acad. Sci. U.S.A.*, *111*, 16268.
[15] Kikuchi, H., Yokota, M., Hisakado, Y., Yang, H., & Kajiyama, T. (2002). *Nat. Mater.*, *1*, 64.

[16] Castles, F., Morris, S. M., Hung, J. M., Qasim, M. M., Wright, A. D., Nosheen, S., Choi, S. S., Outram, B. I., Elston, S. J., Burgess, C., Hill, L., Wilkinson, T. D., & Coles, H. J. (2014). *Nat. Mater.*, *13*, 817.
[17] Wright, D. C., & Mermin, N. D. (1989). *Rev. Mod. Phys.*, *61*, 385.
[18] Kikuchi, H. (2008). *Struct. Bonding*, *128*, 99.
[19] Sihvola, A. (2007). *Metamaterials 1*, 2.
[20] Baba, T. (2008). *Nat. Photonics*, *2*, 465.
[21] Ozbay, E. (2006). *Science 311*, 189.
[22] Martinez, A., Ravnik, M., Lucero, B., Visvanathan, R., Zumer, S., & Smalyukh, I. I. (2014). *Nature Mater.*, *13*, 258.
[23] Zhang, C., Diorio, N., Lavrentovich, O. D., & Jakli, A. (2014). *Nat. Commun.*, *5*, 3302.
[24] Shamid, S., Dhakal, S, & Selinger, J. V. (2013). *Phys. Rev. E*, *87*, 052503.
[25] Chen, D., *et al.* (2014). *Phys. Rev. E*, *89*, 022506.
[26] Ackerman, P. J., Qi, Z., & Smalyukh, I. I. (2012). *Phys. Rev. E*, *86*, 021703.
[27] Senyuk, B., Glugla, D., & Smalyukh, I. I. (2013). *Phys. Rev. E*, *88*, 062507.
[28] Nikkhou, M., Škarabot, M., Čopar, S., Ravnik, M., Žumer, S., & Muševič, I. (2015). *Nature Phys.*, *11*, 183.
[29] Dontabhaktuni, J., Ravnik, M., & Žumer, S. (2014). *Proc. Natl. Acad. Sci. USA*, *111*, 2464.
[30] Yeomans, J. M. (2014). *Nat. Mater.*, *13*, 1004.
[31] Humar, M., & Musevic, I. (2010). *Opt. Expr.*, *18*, 26995.
[32] Pishnyak, O.P., & Lavrentovich, O. D. (2006). *Appl. Phys. Lett.*, *89*, 251103.
[33] , et al. (2012). *Phys. Rev. Lett.*, *109*, 088301.
[34] Stimulak, M., & Ravnik, M. (2014). *Soft Matter*, *10*, 6339.
[35] Cancula, M., Ravnik, M., & Zumer, S. (2014). *Phys. Rev. E*, *90*, 022503.
[36] Cardano, F., Karimi, E., Slussarenko, S., Marrucci, L., de Lisio, C., & Santamato, E. (2012). *Appl. Opt.*, *51*, C1.
[37] Berreman, D. W. (1972). *J. Opt. Soc. Am.*, *62*, 502.
[38] Joannopoulos, J. D., Johnson, S. G., Winn, J. N., & Meade, R. D. (2008). *Photonic Crystals: Molding the Flow of Light, 2nd Ed.*, Princeton Uni. Press.
[39] Johnson, S., & Joannopoulos, J. (2001). *Opt. Express*, *8*, 173.
[40] Taflove, A., & Hagness, S. C. (2005). *Computational Electrodynamics: The Finite-Difference Time-Domain Method,* 3rd ed., Artech House: Norwood, MA.
[41] de Gennes, P. G., & Prost, J. (1993). *The Physics of Liquid Crystals*, 2nd ed., Oxford Science: Oxford.
[42] Ravnik, M., & Zumer, S. (2009). *Liq. Cryst.*, *36*, 1201.
[43] Werner, G. R., & Cary, J. R. (2007). *J. Comput. Phys.*, *226*, 1085.
[44] Hornreich, R. M., Shtrikman, S., & Sommers, C. (1993). *Phys. Rev. E*, *47*, 2067.
[45] Ravnik, M., Alexander, G. P., Yeomans, J. M., & Žumer, S. (2011). *Proc. Natl. Acad. Sci. USA*, *108*, 5188.
[46] Ravnik, M., Alexander, G. P., Yeomans, J. M., & Žumer, S. (2010). *Faraday Discuss.*, *144*, 159.
[47] Johnson, S. G., Ibanescu, M., Skorobogatiy, M. A., Weisberg, O., Joannopoulos, J. D., & Fink, Y. (2002). *Phys. Rev. E*, *65*, 066611.